JOURNAL OF VIROLOGY, July 2009, p. 6416–6428 Vol. 83, No. 13
0022-538X/09/$08.00+0 doi:10.1128/JVI.00445-09

In Vivo Retargeting of Adenovirus Type 5 to αvβ6 Integrin Results in Reduced Hepatotoxicity and Improved Tumor Uptake following Systemic Delivery▽

Lynda Coughlan,[1]* Sabari Vallath,[1] Antonio Saha,[1] Magdalena Flak,[2] Iain A. McNeish,[2] Georges Vassaux,[3] John F. Marshall,[1] Ian R. Hart,[1] and Gareth J. Thomas[1]†

Centre for Tumour Biology, Institute of Cancer, Barts and the London School of Medicine and Dentistry, Charterhouse Square, London EC1M 6BQ, United Kingdom[1]; Centre for Molecular Oncology, Institute of Cancer, Barts and the London School of Medicine and Dentistry, Charterhouse Square, London EC1M 6BQ, United Kingdom[2]; and INSERM U948 Biothérapies Hépatiques and Institut des Maladies de l'Appareil Digestif, CHU Hôtel Dieu, Nantes, France[3]

Received 3 March 2009/Accepted 9 April 2009

A key impediment to successful cancer therapy with adenoviral vectors is the inefficient transduction of malignant tissue in vivo. Compounding this problem is the lack of cancer-specific targets, coupled with a shortage of corresponding high-efficiency ligands, permitting selective retargeting. The epithelial cell-specific integrin αvβ6 represents an attractive target for directed therapy since it is generally not expressed on normal epithelium but is upregulated in numerous carcinomas, where it plays a role in tumor progression. We previously have characterized a high-affinity, αvβ6-selective peptide (A20FMDV2) derived from VP1 of foot-and-mouth disease virus. We generated recombinant adenovirus type 5 (Ad5) fiber knob, incorporating A20FMDV2 in the HI loop, for which we validated the selectivity of binding and functional inhibition of αvβ6. The corresponding αvβ6-retargeted virus Ad5-EGFP$_{A20}$ exhibited up to 50-fold increases in coxsackievirus-and-adenovirus-receptor-independent transduction and up to 480-fold-increased cytotoxicity on a panel of αvβ6-positive human carcinoma lines compared with Ad5-EGFP$_{WT}$. Using an αvβ6-positive (DX3-β6) xenograft model, we observed a ~2-fold enhancement in tumor uptake over Ad5-EGFP$_{WT}$ following systemic delivery. Furthermore, ~5-fold-fewer Ad5-EGFP$_{A20}$ genomes were detected in the liver ($P = 0.0002$), correlating with reduced serum transaminase levels and E1A expression. Warfarin pretreatment, to deplete coagulation factors, did not improve tumor uptake significantly with either virus but did significantly reduce liver sequestration and hepatic toxicity. The ability of Ad5-EGFP$_{A20}$ to improve delivery to αvβ6, combined with its reduced hepatic tropism and toxicity, highlights its potential as a prototype virus for future clinical investigation.

The aim of cancer gene therapy is to achieve targeted delivery of therapeutic transgenes to malignant tissue, with negligible effects on surrounding healthy tissue. Efforts in the development of adenoviruses as therapeutic agents have been persistent. However, several challenges still remain. Inefficient transduction of diseased tissue and the innate hepatotropism and toxicity of adenovirus type 5 (Ad5) in vivo following intravenous delivery represent major issues to be addressed. Additionally, the use of adenoviral vectors for cancer therapy is thought to be incompatible with the broad distribution of the primary adenovirus receptor, the coxsackievirus and adenovirus receptor (CAR), in normal tissues (6). Furthermore, it recently has emerged that human, but not murine, erythrocytes express CAR on their surface, which promotes the sequestration of Ad5 in the circulation and may represent another restriction to efficient tumor delivery in vivo (8).

The predominant adenoviral serotype currently used in gene therapy applications is human Ad5. Ad5 binds to cells through a docking process in which the distal knob domain of the fiber structural protein binds to CAR (6, 23). This is followed by the exposure of an arginine-glycine-aspartate (RGD) motif in the penton base which promotes viral internalization, mediated primarily by αvβ3 and αvβ5 integrins (49). Binding to CAR represents the initial event in cell attachment in vitro, and therefore CAR expression levels long have been thought to be critical in determining the transduction efficiency of Ad5 in vivo. Several studies have reported low expression of CAR in primary carcinoma lines and tumor explants (3, 21, 30, 32, 37), highlighting the necessity for CAR-independent targeting strategies. However, the nonspecific sequestration of Ad5 in the liver remains the major obstacle to achieving high-efficiency tumor targeting following systemic delivery.

A preeminent role for coagulation factors (i.e., FVII, FIX, FX, protein C, and C4BP) in directing liver uptake following systemic delivery has been demonstrated in recent years (36, 41, 48), and hepatocyte transduction now has been shown to be mediated predominantly by a direct Ad5 hexon-FX interaction (22, 48). This discovery has prompted the experimental use of anticoagulants, such as warfarin, in an attempt to avoid liver sequestration, with the aim of increasing the bioavailability of

* Corresponding author. Mailing address: Centre for Tumour Biology, Institute of Cancer, Barts and the London School of Medicine and Dentistry, Charterhouse Square, London EC1M 6BQ, United Kingdom. Phone: 44 020 70140400. Fax: 44 020 70140401. E-mail: l.t.coughlan@qmul.ac.uk.

† Present address: Cancer Sciences Division, University of Southampton School of Medicine, Southampton SO16 6YD, United Kingdom.

▽ Published ahead of print on 15 April 2009.

the virus for the tumor. However, it recently has emerged that coagulation factors may also be required for efficient tumor delivery in vivo and that the depletion of blood factors may in fact preclude successful tumor uptake (16). Accordingly, Ad vector constructs which combine liver detargeting with high-efficiency, CAR-independent gene delivery to cancer-specific receptors are highly desirable.

The epithelial cell-specific integrin αvβ6 generally is undetectable in normal adult tissue but is upregulated significantly in numerous carcinomas, where high expression often correlates with poor prognosis (1, 4, 13). We have shown previously that over 90% of oral squamous cell carcinomas express αvβ6 strongly (35, 45) and that high αvβ6 expression promotes tumor progression (35, 43, 46). Binding to αvβ6 is via the RGD motif in its ligands, which include the latency-associated peptides (LAP) of transforming growth factor β1 (TGF-β1) and TGF-β3 (33), in addition to the VP1 structural protein of foot-and-mouth disease virus (FMDV), for which αvβ6 is a native receptor (20). We have shown that specificity for αvβ6 is dependent on the inclusion of a DLXXL motif in an extended carboxy α-helical loop, with the RGD motif situated at the apex of a hairpin loop domain (10). Functional analysis of known αvβ6 ligands identified a candidate peptide, A20FMDV2, which had high affinity and selective binding to αvβ6 (10). Recent studies have further supported this finding, demonstrating that this peptide forms a highly stable, EDTA-resistant complex with αvβ6 integrin, in a manner analogous to the highly infectious FMDV (11).

Over the past decade, significant attempts to increase the delivery of Ad5 to target tissues have been made by modifying structural tropism determinants. Retargeting strategies have included the insertion of RGD motifs (12), polylysine (pK7) motifs (50) and TAT peptide from human immunodeficiency virus type 1 (26) in attempts to improve delivery to malignant tissue or to the endothelial networks that supply the tumors. The resolution of the crystal structure of the Ad5 knob domain by X-ray crystallography identified the HI loop region as being suitable for peptide incorporation (51), and to date this site has been shown to tolerate the insertion of ligands of up to 83 amino acids with negligible effects on structural integrity (5). In order to redirect the native tropism of Ad5 to αvβ6, we genetically incorporated A20FMDV2 into the HI loop region of the fiber knob domain. We hypothesized that Ad5-EGFP$_{A20}$ would permit significant improvements in selective delivery to αvβ6, both in vitro and in vivo.

Here, we describe the successful subversion of Ad5 infection to αvβ6 expressed on human carcinoma cell lines in vitro and demonstrate that the enhanced transduction observed with Ad5-EGFP$_{A20}$ is CAR independent. We have confirmed that the improved infectivity is due to the insertion of the A20FMDV2 peptide and that cell entry is mediated predominantly through αvβ6 integrin. Additionally, using an αvβ6-positive (DX3-β6) xenograft model, we observed ~2-fold enhancement in tumor uptake over Ad5-EGFP$_{WT}$ in vivo following systemic delivery. Furthermore, ~5-fold-fewer Ad5-EGFP$_{A20}$ genomes were detected in the liver ($P = 0.0002$), correlating with reduced serum transaminase levels and E1A expression. These data show that redirecting Ad5 to αvβ6 can increase tumor delivery while simultaneously limiting hepatotoxicity; this may therefore represent a means of overcoming some of the limitations of current Ad5 therapy.

MATERIALS AND METHODS

Cell lines, yeast strains, and media. Dulbecco's modified Eagle's medium (DMEM), α-MEM, Ham's F-12 medium, and isotonic phosphate-buffered saline (PBS) were supplied by Cancer Research UK (CR-UK) Media Services (South Mimms, Herts). All cell culture media supplied by CR-UK were supplemented with 100 IU penicillin and 100 μg/liter streptomycin. Carcinoma lines used in this study included breast adenocarcinoma line BT-20 (ATCC); ovarian carcinoma line SKOV3ip1 (donated by J. Price, MD Anderson Cancer Center, Houston, TX); head and neck squamous cell carcinoma lines SCC25, TR126, and TR138 (all from CR-UK Cell Services); and αvβ6-expressing lines DX3-B6 and VB6, which have been described previously (29, 43). HEK293 and JH293 were used for amplification and titration of viral constructs, respectively. All cells were cultured in DMEM plus 10% fetal calf serum (Globepharm, Surrey) and 4 mM glutamine (CR-UK Media Services), except BT-20 (α-MEM), SCC25 (Ham's F-12–DMEM), TR138 (Ham's F-12), and VB6, which were grown in keratinocyte growth medium as previously described (43).

The yeast strain *Saccharomyces cerevisiae* YPH857 (ATCC 76628) (*MATα ura3-52 lys2-801 ade2-101 trp1-Δ200 leu2Δ1*) was grown at 30°C in YPD broth (2% [wt/vol] peptone-Y, 1% [wt/vol] yeast extract, and 2% [wt/vol] dextrose) or plated onto YPD supplemented with 1.7% (wt/vol) agar. YPH857 harboring the adenovirus-containing large-construct yeast artificial chromosome plasmid pMB20 (provided by Richard Iggo, University of St. Andrews, United Kingdom) was grown in the synthetic defined dropout medium −HIS (0.17% [wt/vol] yeast nitrogen base, 0.5% [wt/vol] ammonium sulfate, and 2% [wt/vol] dextrose) or plated onto −HIS supplemented with 1.7% (wt/vol) agar. Intermediate recombination derivatives were grown in synthetic dropout medium −HIS −URA or plated onto medium supplemented with 1.7% (wt/vol) agar.

Antibodies. The antibodies used for flow cytometry were anti-αvβ6 monoclonal antibody 53A.2 (generated in house), anti-αvβ3 antibody LM609 (Chemicon), anti-αvβ5 antibody P1F6 (Chemicon), and anti-CAR antibody RmcB (a kind gift from Yaohe Wang, CR-UK). Matched isotype controls were rat immunoglobulin G2a (IgG2a) (Abcam) for 53A.2 and mouse IgG1 (Dako) for all other antibodies. All primary antibodies were used at a final concentration of 10 μg/ml. Fluorescently labeled secondary antibodies used were donkey anti-rat or goat anti-mouse AlexaFluor488 conjugates (Molecular Probes). The αvβ6 function-blocking mouse monoclonal antibody 6.3G9 was used as a positive control for the migration inhibition assay (generously provided by S. Violette, Biogen Idec, MA). Polyclonal rabbit anti-E1A 13S-5 (Santa Cruz) was used for immunostaining of Ad5 E1A in frozen liver tissue, which was carried out in parallel with the relevant isotype control (rabbit IgG1). Fluorescently labeled secondary antibody was goat anti-rabbit AlexaFluor488 (Invitrogen).

Construction of shuttle plasmids for adenovirus genome modifications. Cloning and PCR were performed using standard molecular biology techniques. Shuttle vectors based on the URA integrating shuttle pGV1 (47) were constructed to facilitate recombination with the E3 or fiber region of the Ad5 genome. The construction of a shuttle (pIP5) containing adenoviral sequences flanking the E3 gp19K region has been described previously (31). Enhanced green fluorescent protein (EGFP) was SpeI/XhoI ligated into pIP5 between adenoviral 12.5K and ADP following its compatible NheI/XhoI excision from pEGFP-C1 (Clontech) to create pIP5-EGFP. To generate fiber-modified viruses, adenoviral sequences flanking the site within the fiber (p*IV*) selected for insertion of the αvβ6-targeting A20FMDV2 peptide were cloned from pAdEasy-1 (Stratagene, CA). The upstream and downstream p*IV* fragments (Right/R or Left/L, respectively) were amplified using primers which created an overlapping unique SfoI site at their respective 5′ ends. These overlapping fragments were assembled into the pGV1 shuttle by sequential rounds of subcloning, generating the fiber shuttle pIV_{SfoI}. Terminally phosphorylated, high-pressure liquid chromatography-purified, complementary oligonucleotides corresponding to the cDNA sequence of the αvβ6 binding A20FMDV2 peptide were obtained from Sigma-Genosys. Sense and antisense oligonucleotides (5′-AATGCTGTG CCCAACTTGAGAGGTGACCTTCAAGTGTTGGCTCAAAAGGTGGCAC GGACG-3′ and 5′-CGTCCGTGCCACCTTTTGAGCCAACACTTGAAGGT CACCTCTCAAGTTGGGCACAGCATT-3′, respectively) were annealed together in a 50-μl reaction volume with 1× annealing buffer (2× is 200 mM potassium acetate, 60 mM HEPES-KOH [pH 7.4], and 4 mM magnesium acetate) and were incubated at 95°C for 4 min and then at 70°C for 10 min. This was followed by reductions in temperature of 5°C every 5 min until 4°C was reached. The duplex oligonucleotides were diluted 1:20 and 1 μl of the dilution ligated into 100 ng of SfoI-digested, dephosphorylated pIV_{SfoI} in a final volume of 10 μl.

The ligation reaction mixture was incubated overnight at 16°C, after which 2 μl was used to transform chemically competent DH10B by standard protocols. Constructs were confirmed by sequencing, and the resultant shuttle vector was renamed pIV_{A20}.

Construction of expression vectors and production of recombinant adenoviral knob protein. Adenoviral fiber sequence, corresponding to the knob domain plus the first seven residues of the polylysine repeat motif, was cloned by PCR (using primers which introduced engineered BamHI/HindIII sites) from pAdEasy-1 adenoviral template DNA for $Knob_{WT}$ and from the pIV_{A20} shuttle vector for $Knob_{A20}$. The corresponding PCR products were cloned into pcDNA3.1/V5-HIS-TOPO (Invitrogen) and then BamHI/HindIII digested and subcloned into the pQE30 expression vector as described by Krasnykh et al. (25). Constructs were screened by sequencing to ensure that inserts were in frame with the N-terminal His_6 tag. Optimization of protein expression and purification was carried out at the Protein Isolation and Cloning Lab at CR-UK London Research Institute. Protein expression in *Escherichia coli* SG13009 (pREP4) bacteria harboring the pQE30-$Knob_{WT}$ or pQE30-$Knob_{A20}$ vector was induced on addition of isopropyl-β-D-1-thiogalactopyranoside (IPTG) to a final concentration of 0.1 mM. Soluble recombinant protein was purified under native conditions on Ni-nitrilotriacetic acid agarose columns (Qiagen). The ability of both proteins to form homotrimers was verified by sodium dodecyl sulfate-polyacrylamide gel electrophoresis of boiled and unboiled samples. The concentrations of the purified knobs were determined by the Bradford protein assay (Bio-Rad, Hercules, CA) using bovine IgG as the standard.

Generation of modified Ad5 genomes by homologous recombination in yeast. Modified viral genomes were constructed by two-step homologous recombination in yeast as described by Gagnebin et al. (15). Final-step recombinants were selected on −HIS supplemented with 5-fluoroorotic acid at 0.1 to 0.2% (wt/vol). Generation of Ad5 genomes with modifications in the E3 and fiber gene regions was as follows. YPH857 yeast containing the pMB20 replication-competent Ad5 backbone were freshly streaked onto −HIS agar and incubated overnight at 30°C. A fresh colony was inoculated into 100 ml −HIS broth and incubated for 12 to 24 h at 30°C with aeration, in preparation for lithium acetate transformation the following day using the alkali-cation yeast transformation kit from Q.BIOgene. To create the pMB20-$EGFP_{WT}$ backbone, the E3 gp19K region was replaced with the EGFP transgene using a strategy described elsewhere (19). To create the pMB20-$EGFP_{A20}$ backbone, pMB20-$EGFP_{WT}$ was used as the template for subsequent recombination in the fiber region. Yeast cells were made competent and transformed with linear shuttle DNA. Cells were plated onto −HIS −URA selective agar and incubated at 30°C for 48 to 72 h until transformant colonies appeared. Individual colonies were selected and incubated for 12 to 24 h in 10 ml −HIS −URA broth at 30°C with aeration. Successful integrative recombinants were confirmed by PCR analysis of extracted yeast DNA and were then inoculated into 10 ml −HIS broth and incubated for 12 to 24 h at 30°C with aeration. Following this incubation period, 100 μl of culture was plated onto −HIS plus 5-fluoroorotic acid and incubated for 24 to 48 h at 30°C to select for final-step recombinants. Individual colonies were again selected and screened by PCR following extraction of yeast DNA. Successful constructs were transformed into ElectroMAX DH10B *E. coli* (Invitrogen), amplified with a Large Construct Maxi Kit (Qiagen), and confirmed by sequencing.

Viral production, purification, and titration. Viral genomes were released from their yeast artificial chromosome/bacterial artificial chromosome constructs by PacI digestion and were purified by phenol-chloroform-isoamyl alcohol precipitation followed by centrifugation at 13,000 rpm at room temperature for 5 min. The purified upper fraction was transfected into HEK293 cells using FuGene 6 (Roche). Cells were incubated under standard conditions, (37°C at 5% CO_2) for 3 to 11 days, during which transfection efficiency and cytopathic effect were observed by visualization of EGFP by UV light under a microscope. Viral cultures were expanded, and virus was collected by successive rounds of cesium chloride ultracentrifugation and dialyzed against a solution containing 1 mM $MgCl_2$, 10 mM Tris (pH 7.4), and 150 mM NaCl with 10% glycerol (vol/vol). Viral particle titers were determined by optical density spectrophotometry (optical density at 260 nm). Functional titers were obtained from viral 50% tissue culture infective dose values, read according to the method of Reed and Muench (38). The values for 50% tissue culture infective dose per ml were calculated using the Kärber statistical method $T = 10^{1 + d(S - 0.5)}$, where d is $\log_{10}$ of the dilution and S is the sum of the ratios and values were reduced by 0.7 log, enabling viral titers to be expressed as PFU/ml.

Flow cytometry. Detection of surface receptors by flow cytometry was carried out as described previously (43). Flow cytometry also was used to determine the ability of the modified adenoviral $Knob_{A20}$ protein to bind to αvβ6 on BT-20 cells and to competitively inhibit αvβ6-specific 53A.2 antibody binding. Labeled cells were scanned on an LSR1 flow cytometer (Becton-Dickinson, CA) acquiring 1×10^4 gated events, and results were analyzed using CellQuestPro software.

Migration inhibition assay. Migration assays were carried out, as described previously, to assess the ability of the modified adenoviral protein $Knob_{A20}$ to inhibit αvβ6-dependent cell motility (44). VB6 cells express high levels of αvβ6, and we have shown previously that migration of VB6 cells toward LAP of TGF-β1 is modulated solely through αvβ6 (43). Haptotactic cell migration assays were performed using matrix-coated Transwell filters (8-μm pore size; BD Biosciences). The membrane undersurfaces of three wells were coated with protein control bovine serum albumin (BSA), but all other wells were coated with LAP (0.5 μg/ml in α-MEM) for 1 h at 37°C. All wells were blocked with migration buffer (0.1% BSA in α-MEM) for 30 min at 37°C. Cells were incubated with an αvβ6-inhibitory antibody (6.3G9; 10 μg/ml) or $Knob_{A20}$ protein at the same concentration for 30 min at 4°C prior to seeding. Cells were plated in the upper chamber at a density of 5×10^4 in 100 μl of migration buffer and allowed to migrate for 24 h. Cells which migrated to the lower chamber (including those attached to the lower surface of the membrane) were trypsinized and counted on a Casy 1 counter (Sharfe System GmbH, Germany). Negative controls for inhibition of migration included an isotype IgG1 antibody or $Knob_{WT}$.

In vitro infectivity mediated by the αvβ6 tropism-modified virus, Ad5-$EGFP_{A20}$. The infectivity of Ad5-$EGFP_{A20}$ was compared with that of control virus Ad5-$EGFP_{WT}$ on a panel of αvβ6-expressing human carcinoma cell lines. Characterization of viral entry was achieved through the use of competition assays, using $Knob_{WT}$ or $Knob_{A20}$ to inhibit viral infection and a function-blocking antibody to αvβ6 integrin (53A.2) in parallel. Further function-blocking experiments were carried out using inhibitors to integrins required for native adenoviral internalization (αvβ3/αvβ5) in order to demonstrate that the tropism of Ad5-$EGFP_{A20}$ was predominantly through αvβ6 and therefore was independent of αvβ3/αvβ5 expression. Confluent monolayers were preincubated with an excess of $Knob_{WT}$, $Knob_{A20}$, or the relevant antibodies (10 μg/ml) for 1 h at 4°C. Without washing, Ad5-$EGFP_{WT}$ or Ad5-$EGFP_{A20}$ was added to cells at a multiplicity of infection (MOI) of 10. Incubation was carried out at 4°C for 1 h to promote virus binding without internalization, monolayers washed twice in cold PBS to remove unbound virus, and cells covered with prewarmed complete medium and incubated at 37°C for 22 h to allow EGFP transgene expression. Viral EGFP gene transfer and competition gene transfer assays were quantified by acquisition of EGFP fluorescence in FL1-H by flow cytometry.

Cytotoxicity assays. Cell viability following viral infection was estimated using a 3-2,5-diphenyltetrazolium bromide (MTT) (Sigma-Aldrich, Poole, United Kingdom) assay. Carcinoma cells (2×10^5) were seeded in 24-well plates and infected with 10-fold serial dilutions of virus (MOIs of 0.0001 to 100) in medium with 5% fetal calf serum. At 120 h postinfection, an MTT assay was carried out and absorbance read at 560 nm in a 96-well plate with an Opsys MR microplate reader (Dynex Technologies Ltd., West Sussex, United Kingdom). Cell viability assays were carried out in triplicate and repeated on three independent occasions.

In vivo studies. DX3-β6 cells (4×10^6) were implanted subcutaneously into the shoulders of CD1 nude female mice. When tumors reached approximately 125 mm^3 (~3 weeks), mice were injected with PBS, Ad5-$EGFP_{WT}$, or Ad5-$EGFP_{A20}$ (5×10^{10} viral particles per mouse) by intravenous tail vein injection. In order to deplete vitamin K-dependent coagulation factors, identical but separate groups were injected subcutaneously with 133 μg warfarin (Sigma) dissolved in peanut oil (Sigma) at days −1 and −3 prior to viral administration (36). Mice were killed at 72 h postinfection and tumors/organs harvested for analysis. Liver transaminase enzymes alanine aminotransferase (ALT) and aspartame aminotransferase (AST) were quantified from 150 μl of mouse serum at Axiom Veterinary Laboratories (Devon, United Kingdom). Viral and total genomic DNAs were obtained from tissue using the QIAamp DNA mini kit (Qiagen, United Kingdom) and 20 ng of total DNA subjected to fluorogenic TaqMan real-time quantitative PCR (qPCR) using the Applied Biosystems 7500 real-time PCR system. TaqMan reactions were performed in triplicate, on two separate occasions, using primers for the hexon region of the genome (forward, 5′-AGC GCGCGAATAAACTGCT-3′, and reverse, 5′-AGGAGACCACTGCCATGTT GT-3′ [Sigma]) and a probe from Applied Biosystems (hexon probe FAM-CC GCCGCTCCGTCCTGCA-MGB). Total adenoviral genomes were calculated using a standard curve of 10^1 to 10^9 viral genomes, and data were analyzed using Sequence Detection software v1.3 (Applied Biosystems).

Immunohistochemistry. Immediately after necropsy, sections of liver tissue were embedded in O.C.T (Tissue-Tek) and frozen at −80°C. Sections of 5 μm were cut using a Cryotom electronic cryostat (Thermo Electron Corporation) and two sections loaded onto charged slides (both Tissue-Tek). Sections were stained for E1A expression using a rabbit polyclonal antibody, 13 S-5 (Santa Cruz), as follows. Precut frozen sections were fixed in ice-cold acetone for 10

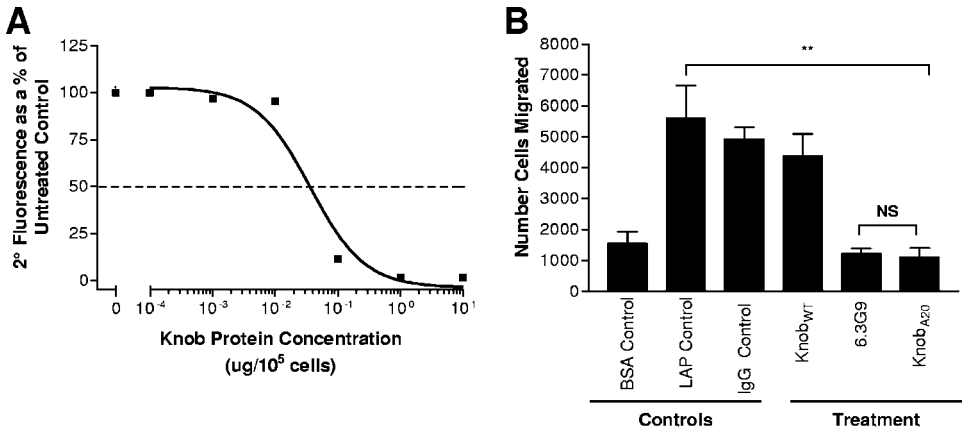

FIG. 1. Characterization of A20FMDV2 peptide function within the recombinant $Knob_{A20}$ protein. (A) $Knob_{A20}$ binds to αvβ6 on BT-20 cells and competitively inhibits the binding of an αvβ6-specific antibody (53A.2) in a dose-dependent manner. Cells were incubated with increasing concentrations of $Knob_{A20}$ (0.0001 to 10 μg protein/10^5 cells). 53A.2 was added and binding detected by flow cytometry using a donkey anti-rat antibody conjugated to AlexaFluor488. Cells not treated with recombinant knob protein were taken as having 100% fluorescence and the fluorescence of treated samples expressed as a percentage of this. (B) $Knob_{A20}$ abrogates the αvβ6-dependent migration of VB6 cells toward LAP of TGF-β1. A BSA protein control (cells untreated with LAP) represents background cell migration, whereas cells treated with LAP alone represent the level of αvβ6-dependent migration. An IgG1 isotype control antibody was included as a negative control. Cells were treated with $Knob_{WT}$, $Knob_{A20}$, or a function-blocking antibody to αvβ6 (6.3G9), a known inhibitor of αvβ6-dependent cell migration. All antibodies and recombinant proteins were used at a final concentration of 10 μg/ml. Data represent the mean ± SD for triplicate samples and are representative of two independent experiments carried out within a single plate. Statistical significance was determined using the unpaired Student *t* test comparing the means of two samples (**, $P < 0.01$; no bars, SD values smaller than the symbol used; NS, not statistically significant [$P > 0.05$]).

min, rinsed in deionized H_2O, and blocked for 30 min in 10% normal goat serum (Sigma, United Kingdom). Primary antibody 13 S-5 (Santa Cruz) or a rabbit isotype control (IgG1; Dako) diluted 1:100 in PBS plus Tween 0.05% was added and sections incubated for 1 h at room temperature. Sections were washed several times in PBS plus Tween 0.05%, after which a fluorescent secondary, goat anti-rabbit antibody (AlexaFluor488; Invitrogen) was added and left for 1 h at a final dilution of 1:200. Sections were washed and mounted with VectaShield+DAPI (Vector Laboratories, United Kingdom), coverslips added, and slides allowed to dry overnight. Immunofluorescence was visualized using a Zeiss laser scanning microscope (LSM 510META) and pictures captured using LSM 5 software, version 3.2 (Zeiss, Germany).

Statistical analysis. All graphs, dose-response curves, and statistical analyses were generated with GraphPad Prism version 3.03 (GraphPad Software, San Diego, CA). The unpaired Student *t* test was used to compare means between two samples. For nonlinear regression analysis, the unpaired Student *t* test was used to demonstrate the significance of the differences in 50% effective concentrations (EC_{50} values) for each virus. A *P* value of <0.05 was considered to be statistically significant. Figures show representative examples of independent repeats. In vitro data are expressed as the mean ± standard deviation (SD) and in vivo data as the mean ± standard error of the mean (SEM).

RESULTS

The A20FMDV2 peptide within the Ad5 knob domain binds to and abrogates the function of αvβ6 in vitro. We have shown previously that the specificity of the A20FMDV2 peptide for αvβ6 is dependent on the formation of a critical post-RGD, C-terminal α-helical loop (10). To model whether the A20FMDV2 peptide could assume its critical helical conformation within the structural constraints of the adenoviral knob protein, we used Agadir software (http://www.embl-heidelberg.de/Services/serrano/agadir/agadir-start.html) to predict the potential helical propensity of A20FMDV2 within $Knob_{A20}$ (data not shown). The algorithm prediction was favorable; however, the insertion of targeting ligands into the HI loop does not automatically correlate with the retention of their function in the context of the trimeric fiber. We constructed recombinant $Knob_{A20}$ to address these issues and performed a number of assays to confirm that the A20FMDV2 peptide retained its function.

In vitro assays confirmed the ability of $Knob_{A20}$ protein to mediate αvβ6 binding and to abrogate αvβ6-dependent function. Using BT-20 cells (with high levels of αvβ6 but low levels of CAR), we tested the ability of $Knob_{A20}$ (0.0001 μg to 10 μg/10^5 cells) to bind to αvβ6 and competitively inhibit the subsequent binding of an anti-αvβ6 MAb, 53A.2 (Fig. 1A). Levels of bound 53A.2 were detected by flow cytometry and secondary antibody fluorescence expressed as a percentage of that for the untreated control cells (taken as 100%). $Knob_{A20}$ exhibited dose-dependent inhibition of αvβ6-specific antibody binding, with 50% maximal inhibition at 0.03 μg/10^5 cells (Fig. 1A). $Knob_{WT}$ was included as a control used at a high concentration (100 μg/10^5 cells) but was unable to block 53A.2 binding and did not differ from untreated cells ($P = 0.498$; data not shown).

The ability of $Knob_{A20}$ to functionally inhibit αvβ6-dependent VB6 cell migration toward the LAP of TGF-β1 also was confirmed (Fig. 1B). VB6 cells have been modified to express high levels of αvβ6 and migrate toward LAP using only αvβ6 (43, 44). $Knob_{A20}$ significantly inhibited VB6 cell migration toward LAP ($P = 0.002$) as efficiently as an αvβ6-inhibitory antibody (6.3G9), whereas $Knob_{WT}$, used at an equal concentration, produced no significant effect ($P = 0.173$). These data confirmed that the A20FMDV2 insertion, within the structural constraints of the adenovirus Knob protein, was functional with respect to αvβ6 binding and abrogation of αvβ6 function.

Analysis of a panel of human carcinoma cell lines for CAR and αvβ6 expression. Carcinoma lines were analyzed by flow cytometry for their cell surface expression of CAR, αvβ6, and αvβ3/αvβ5 integrins (Table 1). In contrast with the high level

TABLE 1. Levels of surface receptor expression[a]

Cells	CAR		αvβ3		αvβ5		αvβ6	
	% Positive	Geometric mean fluorescence	% Positive	Geometric mean fluorescence	% Positive	Geometric mean fluorescence	% Positive	Geometric mean fluorescence
BT20	5.01	14.79	1.05	0.10	93.00	15.01	96.35	33.08
DX3-β6	9.07	12.74	97.38	21.92	88.97	17.69	96.55	156.56
TR126	3.96	46.52	1.63	1.36	1.56	4.00	94.82	72.28
SKOV3ip1	56.91	37.30	6.45	11.11	32.72	29.15	50.11	17.09
TR138	56.39	71.17	ND	ND	ND	ND	94.16	115.86
SCC25	96.55	37.22	62.08	20.54	9.91	4.15	97.42	72.19

[a] Geometric mean fluorescence and percent positive statistics were collected using single-parameter histograms (FL1-H). Negative control isotype IgG fluorescence values were subtracted from the geometric mean fluorescence of the test antibody (mouse IgG1, anti-CAR [RmcB], anti-αvβ3 [LM609], and anti-αvβ5 [P1F6]; rat IgG2a, anti-αvβ6 [53A.2]). ND, not determined.

of αvβ6 expression found in many carcinomas, CAR expression is reported to be downregulated in tumors in vivo. In order to reflect this observation when analyzing infectivity, a panel of cell lines with high αvβ6 expression but differential expression of CAR and αvβ3/αvβ5 was chosen for further investigation. Flow cytometry analysis demonstrated that CAR expression detected in this panel of cell lines was in the order TR126 < BT-20 < DX3-β6 < TR138 = SKOV3ip1 < SCC25.

Ad5-EGFP$_{A20}$ can enhance significantly the infection of αvβ6-expressing carcinoma cell lines in a CAR-independent manner. We assessed the capacity of fiber-modified adenovirus Ad5-EGFP$_{A20}$ to target αvβ6 integrin successfully, circumventing the dependence on CAR for gene delivery. Flow cytometry was used to determine the ability of Ad5-EGFP$_{A20}$ to improve delivery to a panel of αvβ6-positive human carcinoma lines relative to Ad5-EGFP$_{WT}$ (Fig. 2A). Infectivity is represented as the percentage of cells expressing EGFP and was quantified at 22 h postinfection. The αvβ6-retargeted virus Ad5-EGFP$_{A20}$ demonstrated significantly improved transduction efficiency at an MOI of 10 compared with Ad5-EGFP$_{WT}$ in all six lines ($P < 0.0001$ for all). We observed a 50-fold increase in transduction in BT-20 cells infected with Ad5-EGFP$_{A20}$, which contrasted with the poor efficiency of Ad5-EGFP$_{WT}$ in mediating infection under identical conditions. Ad5-EGFP$_{A20}$ also enhanced transduction significantly in two further low-CAR cell lines compared with the unmodified control, Ad5-EGFP$_{WT}$, with gene transfer increased 50-fold and 10-fold for DX3-β6 and TR126, respectively. Furthermore, Ad5-EGFP$_{A20}$ also infected cells with moderate to high CAR levels with better efficiency than Ad5-EGFP$_{WT}$, increasing infectivity 5-fold, 2-fold, and 1.5-fold (SKOV3ip1, TR138, and SCC25, respectively). These data confirmed that the insertion of the A20FMDV2 peptide enhances the infectivity of αvβ6-positive cells lines, some of which previously were refractory to infection with Ad5-EGFP$_{WT}$.

The use of recombinant knob protein to block the infection of a virus from which it was derived is a well-established assay. The 50% inhibitory concentration for the modified protein Knob$_{A20}$ was calculated by preincubating BT-20 cells with increasing concentrations of Knob$_{A20}$ (0.0001 to 10 μg/10^5 cells) followed by superinfection with Ad5-EGFP$_{A20}$ (Fig. 2B). BT-20 cells were chosen due to their high αvβ6 status and their almost negative CAR expression (see Table.1). We also included an excess of Knob$_{WT}$ (100 μg/10^5 cells) as a control in this experiment and showed that it had no discernible effect ($P = 0.969$; data not shown). The ability of Knob$_{A20}$ to abrogate infection with Ad5-EGFP$_{A20}$ in a dose-dependent manner (50% inhibitory concentration of 0.008 μg/10^5 cells) confirmed that the infectivity enhancement we observed was conferred by the A20FMDV2 insertion.

In order to characterize the altered tropism further, infectivity experiments were performed in the presence of various inhibitors. The effects of Knob$_{WT}$ and Knob$_{A20}$ on infection were assessed alongside those of a function-blocking antibody to αvβ6 (Fig. 2C). Preincubation with 10 μg/ml of either Knob$_{A20}$ or 53A.2 significantly reduced Ad5-EGFP$_{A20}$ infection in the three low-expressing CAR cell lines BT20, TR126, and DX3-β6 ($P < 0.0001$ for both inhibitors on all three cell lines) and reduced infection to baseline Ad5-EGFP$_{WT}$ levels on three further lines which had moderate to high CAR surface expression (data not shown). Knob$_{WT}$ used at the same concentration did not affect Ad5-EGFP$_{A20}$ infection ($P > 0.05$; data not shown). Therefore, the ability of Ad5-EGFP$_{A20}$ to infect low-expressing CAR lines or to support efficient infection in the presence of an excess of Knob$_{WT}$ confirms that the αvβ6-retargeted virus Ad5-EGFP$_{A20}$ is capable of high-efficiency, CAR-independent attachment. Moreover, through the use of αvβ6-specific function-blocking assays, we have demonstrated that αvβ6 acts as a high-efficiency surrogate receptor for cell entry.

We have shown previously that the A20FMDV2 peptide does not interact with αvβ3 and αvβ5 integrins (10). However, to ensure that Ad5-EGFP$_{A20}$ infection was independent of either of these integrins, we carried out further infectivity experiments on DX3-β6 cells, using function-blocking antibodies to αvβ6 in parallel with αvβ3/αvβ5 inhibitors (Fig. 2D). Ad5-EGFP$_{WT}$, included as a control, gave results identical to those obtained previously (Fig. 2A). Clearly, neither αvβ3 nor αvβ5 plays any significant role in facilitating Ad5-EGFP$_{A20}$ entry to these cells. Simultaneous inhibition of both integrins resulted in a ~9% reduction in Ad5-EGFP$_{A20}$ mediated transduction, whereas inhibition of αvβ6 resulted in a 76% reduction in transduction (Fig. 2D). These data confirm that αvβ6 is the primary determinant for Ad5-EGFP$_{A20}$ entry.

Ad5-EGFP$_{A20}$ displays enhanced cytotoxicity on cell lines which have high αvβ6 expression. Comparative cytotoxicity profiles (MTT assay) for Ad5-EGFP$_{WT}$ and Ad5-EGFP$_{A20}$ on each of the carcinoma cell lines used in this study are shown in Fig. 3A to F. Ad5-EGFP$_{A20}$ exhibited significantly increased cytotoxicity on all lines tested, except for SCC25. The EC$_{50}$

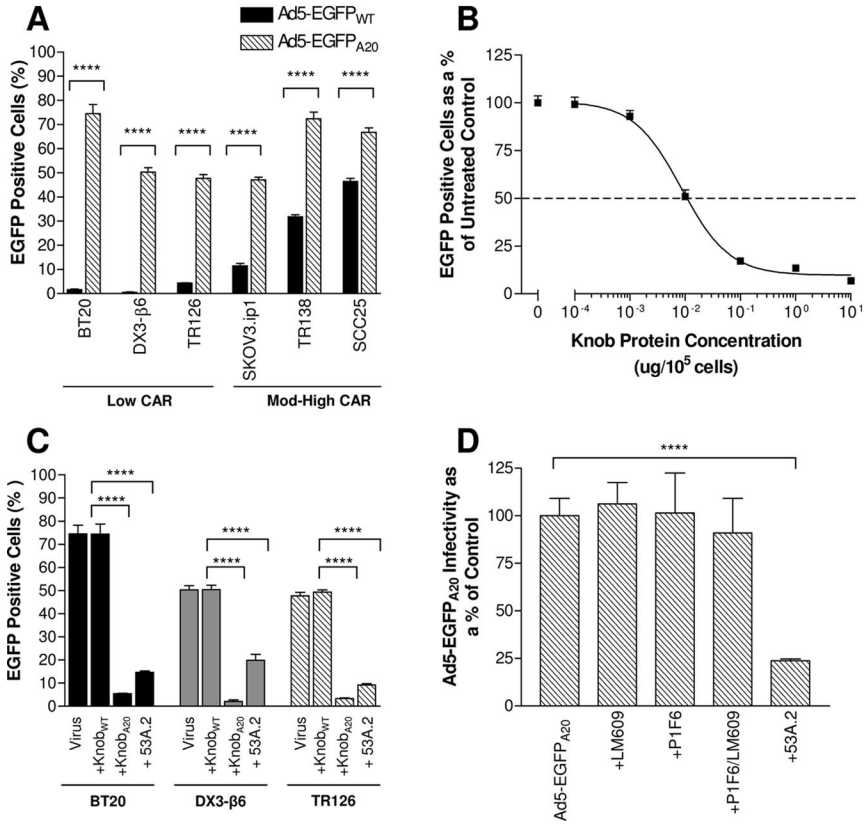

FIG. 2. Characterization of Ad5-EGFP$_{A20}$ infectivity on αvβ6-expressing carcinoma cell lines. (A) Histogram showing the comparative infectivities of Ad5-EGFP$_{WT}$ and Ad5-EGFP$_{A20}$ on a panel of human carcinoma cell lines. Histograms show absolute values for the percentage of cells positive for adenoviral EGFP gene transfer following infection at an MOI of 10, quantified at 22 h postinfection by flow cytometry in FL1-H, acquiring 1×10^4 gated events. Low CAR is defined as <10% and moderate to high (Mod-High) CAR as >50% cells staining positive in flow cytometry (Table 1) (B) Competitive inhibition assay using Knob$_{A20}$ to block Ad5-EGFP$_{A20}$-mediated infectivity, confirming that A20FMDV2 confers enhanced transduction. Cells were preincubated with increasing concentrations of Knob$_{A20}$ protein (0.0001 to 10 μg/10^5 cells), after which they were infected with Ad5-EGFP$_{A20}$ at an MOI of 10 and the percentage EGFP positive cells quantified by flow cytometry. The 50% maximal inhibition value for Knob$_{A20}$ on subsequent Ad5-EGFP$_{A20}$ infection was determined to be 0.008 μg/10^5 cells. (C) Characterization of Ad5-EGFP$_{A20}$-mediated transduction. BT-20, DX3-B6, and TR126 cells were infected following preincubation with Knob$_{WT}$, Knob$_{A20}$, or an anti-αvβ6 antibody (53A.2). (D) Ad5-EGFP$_{A20}$-mediated infection is via αvβ6 and is independent of αvβ3/αvβ5 integrins. A competitive inhibition assay was carried out with DX3-β6 cells in the presence or absence of function-blocking antibodies to αvβ3 (LM609), αvβ5 (P1F6), both simultaneously (LM609/P1F6) or anti-αvβ6 53A.2. Cells were infected with either Ad5-EGFP$_{WT}$ (negative with <1.0% cells infected) or Ad5-EGFP$_{A20}$ at an MOI of 10. Ad5-EGFP$_{A20}$ is expressed as 100% positive, with all other values relative to this. All antibodies and recombinant proteins were used at a final concentration of 10 μg/ml. Data represent the mean ± SD for triplicate samples and are representative of three independent experiments. Statistical significance was determined using the unpaired Student *t* test comparing the means of two samples (****, $P < 0.0001$; no bars, SD values smaller than the symbol used).

values obtained at 120 h postinfection are listed in Table 2. An approximately 480-fold increase in cytotoxicity was observed for BT-20 cells infected with Ad5-EGFP$_{A20}$ compared with Ad5-EGFP$_{WT}$ (Fig. 3A), a ~90-fold increase for DX3-β6 (Fig. 3B), ~17-fold for TR126 and SKOV3ip1, and ~33-fold for TR138 (Fig. 3C, D, and E, respectively). Differences between both viruses on SCC25 cells, which express high levels of CAR, were not found to be significant (Fig. 3F). The *P* values displayed in Fig. 3 refer to the difference between the EC_{50} values for each virus.

Ad5-EGFP$_{A20}$ displays improved tumor uptake following systemic delivery. We compared the in vivo tumor-targeting efficiency of Ad5-EGFP$_{WT}$ and Ad5-EGFP$_{A20}$ using a subcutaneous xenograft model, DX3-β6 (low CAR and high αvβ6), implanted into the right shoulders of CD1 nude mice. A single dose of 5×10^{10} viral particles [vp]/mouse was administered by tail vein injection to separate groups which had or had not received warfarin pretreatment. Three days later all mice were killed, tumors excised, and absolute viral genome levels detected by fluorogenic quantitative real-time PCR (Fig. 4A). Mice not treated with warfarin showed enhanced tumor uptake of Ad5-EGFP$_{A20}$ compared with Ad5-EGFP$_{WT}$ (~2.1-fold increase in viral genomes detected). In the warfarin-treated groups, there was an improvement in tumor delivery of Ad5-EGFP$_{WT}$ (~1.4-fold increase) but a reduced uptake of Ad5-EGFP$_{A20}$ (~1.6-fold decrease) compared with the corresponding non-warfarin-treated groups (Fig. 4A).

Ad5-EGFP$_{A20}$ displays reduced liver sequestration following systemic delivery. Absolute numbers of viral genomes in the liver, for both the non-warfarin-treated and warfarin-treated groups, were measured (Fig. 4B). In non-warfarin-treated mice there was significant uptake of Ad5-EGFP$_{WT}$ in the liver.

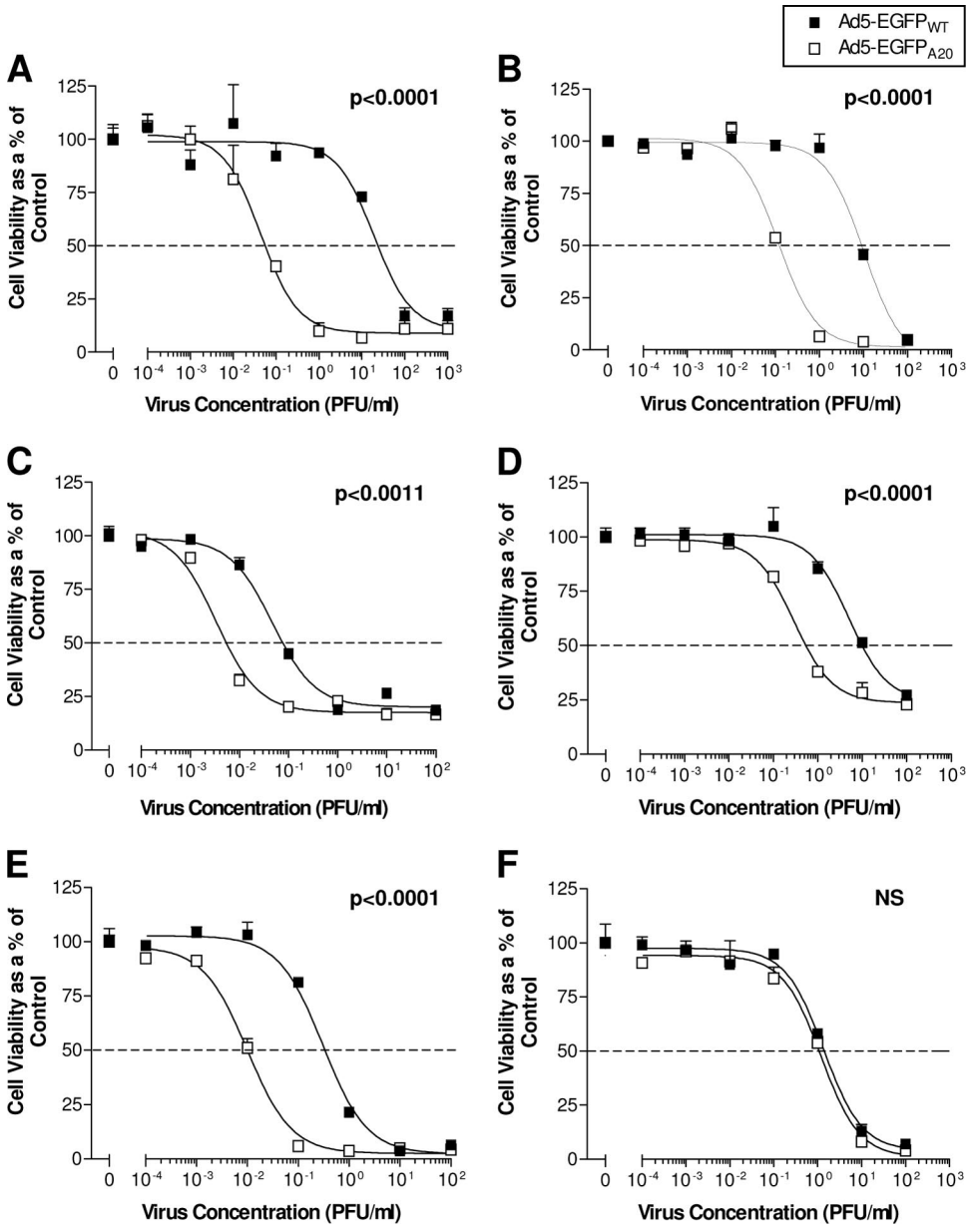

FIG. 3. In vitro cytotoxicity profiles of Ad5-EGFP$_{A20}$ was compared with Ad5-EGFP$_{WT}$ on αvβ6-positive carcinoma lines. A panel of six carcinoma cell lines was infected in parallel with either Ad5-EGFP$_{WT}$ or Ad5-EGFP$_{A20}$ (MOI of 0.0001 to 100 PFU/cell). (A) BT-20; (B) DX3-β6; (C) TR126; (D) SKOV3.ip1; (E) TR138; (F) SCC25. Cell survival was determined by MTT assay at 120 h postinfection, and EC_{50} values for the dose-response curves are displayed in Table 2. Mean percent survival was expressed as a percentage of uninfected cells ($n = 3$); bars indicate SD (no bars represent SD values smaller than the symbol used). The unpaired Student t test was used to demonstrate the significance of the difference in EC_{50} values for each virus (NS, not statistically significant [$P > 0.05$]). Cytotoxicity profiles shown are representative of three independent repeat experiments carried out in triplicate on different occasions.

TABLE 2. EC_{50} values[a]

Virus	EC_{50} (PFU/cell) with:					
	BT-20	DX3-β6	TR126	SKOV3ip1	TR138	SCC25
Ad5-EGFP$_{WT}$	19.13	10.33	0.05	5.02	0.3	1.37
Ad5-EGFP$_{A20}$	0.04	0.12	0.003	0.29	0.009	1.2

[a] Viability was assessed by MTT assay and results analyzed by nonlinear regression fitted to a sigmoidal curve.

However, in comparison, and rather unexpectedly, we observed ~5-fold-fewer Ad5-EGFP$_{A20}$ genomes in the liver ($P = 0.0002$). Immunostaining of frozen sections also demonstrated a clear reduction in the level of E1A expression in the livers of the Ad5-EGFP$_{A20}$ group (Fig. 4B, inset).

A significant reduction in E1A expression, in addition to an overall reduction in viral genome levels (~9-fold; $P < 0.0001$), was found in the Ad5-EGFP$_{WT}$ group subjected to warfarin pretreatment. However, warfarin had a more striking effect on

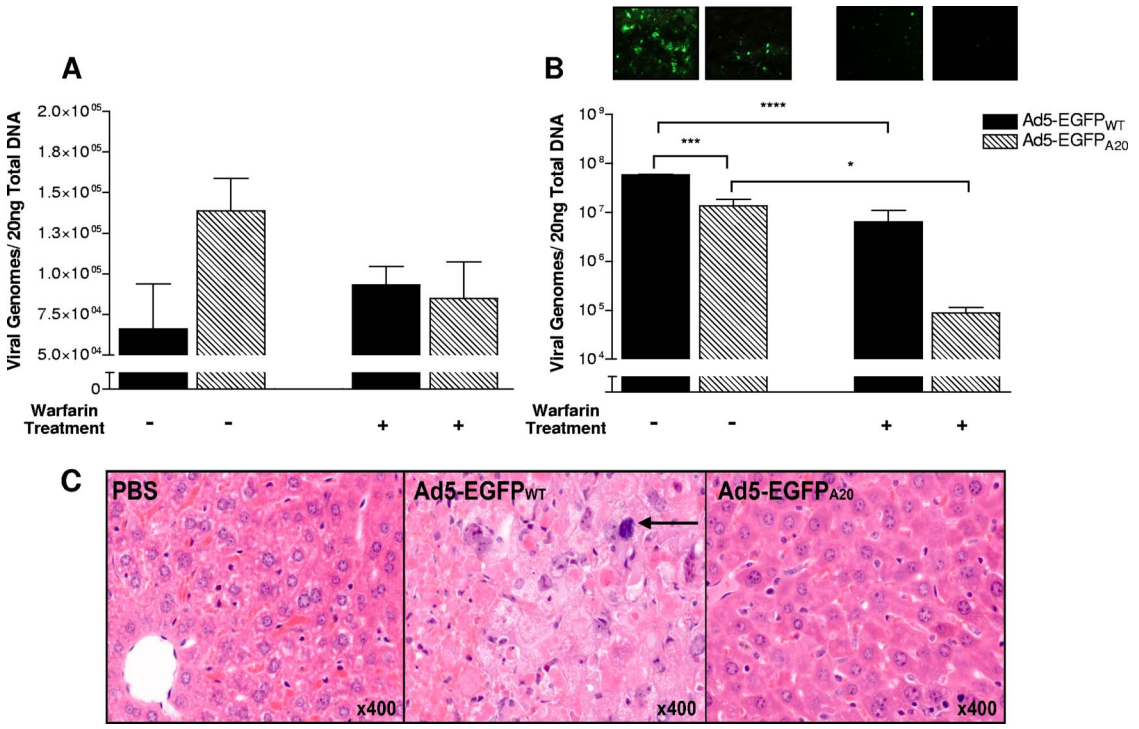

FIG. 4. Quantification of viral genomes in tumor and liver and liver histology. (A) CD1 nude female mice bearing DX3-β6 xenografts were injected with either PBS, Ad5-EGFP$_{WT}$, or Ad5-EGFP$_{A20}$ (5×10^{10} vp/mouse) by intravenous tail vein injection without (−) or with (+) a predose of warfarin (133 μg) at days 3 and 1 prior to virus administration. Mice were killed after 72 h, necropsy performed, and DNA extracted from DX3-β6 tumors. Absolute viral genomes were quantified by TaqMan real-time qPCR using a probe to detect the hexon region of the genome. (B) DNA was extracted from mouse livers and absolute viral genomes quantified as before. Inset, E1A staining on frozen liver sections (magnification, ×20). Data presented in both panels A and B represent the mean ± SEM ($n = 4$ or 5 mice) for triplicate qPCR samples and are representative of two independent qPCR experiments. Statistical significance was determined using the unpaired Student t test comparing the means of two samples (*, $P < 0.05$; ***, $P < 0.001$; ****, $P < 0.0001$). (C) Hematoxylin and eosin staining of liver sections from non-warfarin-treated animals. From left to right: PBS control, Ad5-EGFP$_{WT}$, and Ad5-EGFP$_{A20}$. In the central section, an arrow indicates an enlarged, hyperchromatic hepatocyte nucleus. Much of this section shows hepatocyte necrosis with loss of cellular and nuclear definition.

the liver uptake of Ad5-EGFP$_{A20}$, with viral genomes reduced by ~160-fold ($P = 0.035$) compared with the untreated Ad5-EGFP$_{A20}$ group (Fig. 4B). This was confirmed by the absence of E1A expression, detected by immunostaining, in frozen liver sections (Fig. 4B, inset).

Hematoxylin and eosin staining of liver sections also revealed distinct histological differences between non-warfarin-treated Ad5-EGFP$_{WT}$ and Ad5-EGFP$_{A20}$ groups (Fig. 4C), supporting the data shown in Fig. 4B. The livers of Ad5-EGFP$_{WT}$-treated mice showed prominent hepatocyte atypia and necrosis. However, the livers of mice which had received the Ad5-EGFP$_{A20}$ treatment more closely resembled those of mice in the PBS control group.

Systemic delivery of Ad5-EGFP$_{A20}$ is associated with significantly reduced toxicity in vivo. The hepatotoxicity induced following systemic delivery of replicating adenoviruses in murine models is dose limiting (2). Therefore, we compared the toxicities induced by intravenous delivery of Ad5-EGFP$_{WT}$ and Ad5-EGFP$_{A20}$ (5×10^{10} vp/mouse), assessing percent body weight variation on a daily basis and serum transaminase (ALT and AST) levels at the time of death (Fig. 5A to F). In non-warfarin-treated mice, we observed significant changes in body weight variation between the Ad5-EGFP$_{WT}$ and Ad5-EGFP$_{A20}$ groups (Fig. 5A). Variation in the Ad5-EGFP$_{WT}$ group on day 2 was −8.2% ± 1.3%, compared with −4.0% ± 1.4% for the Ad5-EGFP$_{A20}$ group ($P = 0.003$), and at this time point only the Ad5-EGFP$_{WT}$ group differed statistically from the PBS control group ($P = 0.0006$). On day 3, the percent weight variation in the Ad5-EGFP$_{WT}$ group was −11.7% ± 2.2%, differing significantly from that of the Ad5-EGFP$_{A20}$ group ($P = 0.004$), which remained largely unchanged from day 2 at −3.8% ± 3.2%. In warfarin-treated groups no significant weight variation was observed at any time point (Fig. 5B), except for the Ad5-EGFP$_{WT}$ group on day 1 compared with the PBS control group ($P = 0.031$).

In the non-warfarin-treated Ad5-EGFP$_{WT}$ group, there were significant elevations in serum ALT (Fig. 5C) and AST levels (Fig. 5E), which were substantially lower in the Ad5-EGFP$_{A20}$ group ($P = 0.025$ and $P = 0.0003$, for ALT and AST, respectively). These data corroborated previous results (Fig. 4B and C), confirming that Ad5-EGFP$_{A20}$ has reduced hepatotoxicity in vivo. As warfarin pretreatment can reduce the hepatic uptake of wild-type Ad5 significantly, we also analyzed serum levels of ALT (Fig. 5D) and AST (Fig. 5F) in these treated groups. Compared with non-warfarin-treated groups, pretreatment with warfarin significantly reduced ALT and AST levels for the Ad5-EGFP$_{WT}$ group (ALT, ~15-fold reduction [$P = 0.007$]; AST, ~20-fold [$P < 0.0001$]).

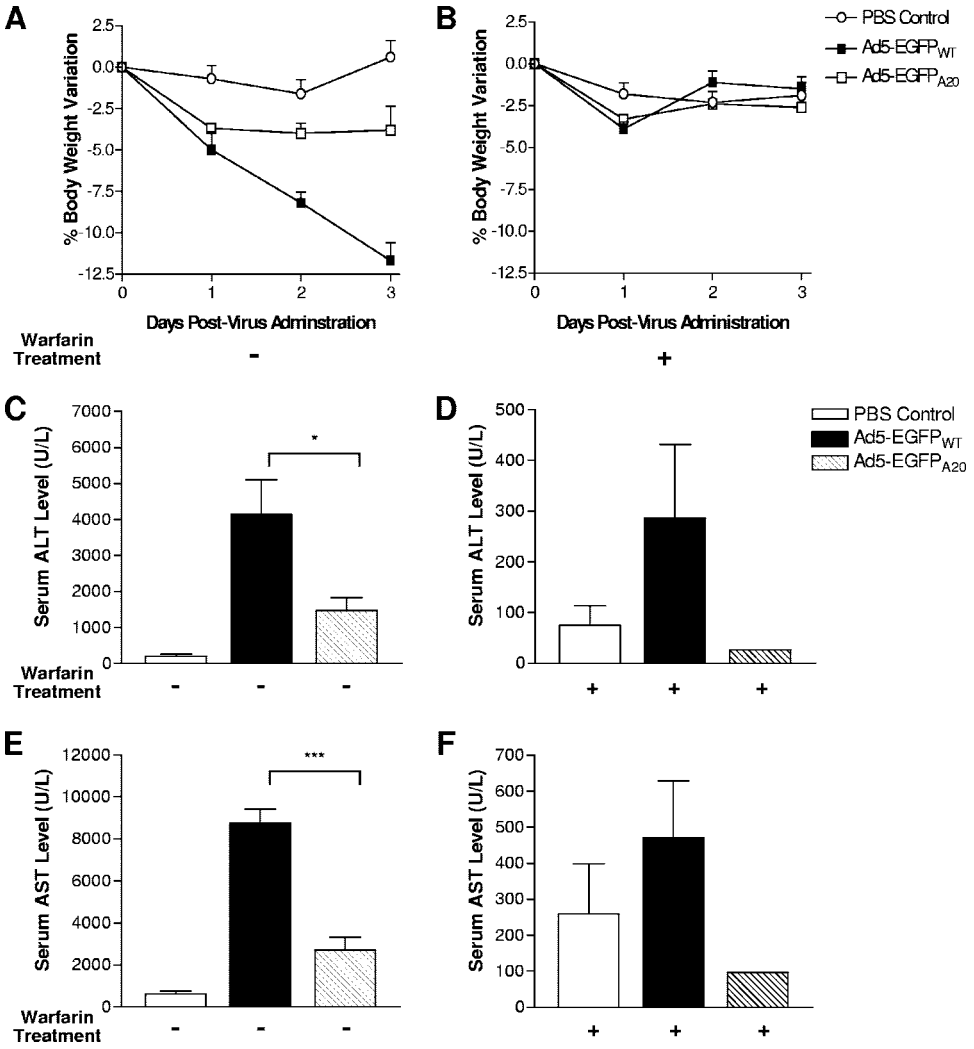

FIG. 5. Determination of toxicity following systemic administration of virus. (A) Percent body weight variation for mouse groups which received intravenous delivery of PBS, Ad5-EGFP$_{WT}$, or Ad5-EGFP$_{A20}$ (5×10^{10} vp/mouse). (B) Percent body weight variation for mouse groups as described for panel A, which received a warfarin predose at days −1 and −3. (C) Blood samples were obtained immediately postmortem (72 h after virus administration) and serum ALT levels were quantified for each of the non-warfarin-treated groups (PBS, Ad5-EGFP$_{WT}$, and Ad5-EGFP$_{A20}$). (D) Serum ALT levels were quantified for warfarin-pretreated cohorts as described for panel C. (E) Serum AST levels were quantified for all non-warfarin-treated groups (PBS, Ad5-EGFP$_{WT}$, and Ad5-EGFP$_{A20}$). (F) Serum AST levels were quantified for all groups which received a warfarin predose, as described for panel E. Data represent the mean ± SEM ($n = 4$ or 5 mice). Statistical significance was determined using the unpaired Student t test comparing the means of two samples (*, $P < 0.05$; ***, $P < 0.001$).

Altered distribution of Ad5-EGFP$_{A20}$ in spleen and lung compared with Ad5-EGFP$_{WT}$. We observed a significantly altered distribution of Ad5-EGFP$_{A20}$ and Ad5-EGFP$_{WT}$ in the spleens and lungs (Fig. 6A and B, respectively) of DX3-β6 tumor-bearing mice. In non-warfarin-treated groups, Ad5-EGFP$_{WT}$ genome levels in the spleen (Fig. 6A) were significantly higher than Ad5-EGFP$_{A20}$ genome levels (~3-fold; $P = 0.046$), although warfarin pretreatment reduced this accumulation (~7-fold; $P = 0.012$). Warfarin pretreatment of Ad5-EGFP$_{WT}$ succeeded in reducing uptake in the spleen only to a level equivalent to that for Ad5-EGFP$_{A20}$ alone ($P = 0.316$). Moreover, warfarin did not further enhance the splenic detargeting already observed with Ad5-EGFP$_{A20}$ ($P = 0.206$).

In addition to the reduced splenic uptake of Ad5-EGFP$_{A20}$, we also observed differential genome numbers in the lung compared to Ad5-EGFP$_{WT}$ in non-warfarin-treated animals (Fig. 6B). Ad5-EGFP$_{A20}$ also appears to naturally be detargeted from murine lung tissue (~9-fold reduction; $P < 0.0001$) compared with Ad5-EGFP$_{WT}$. Since Ad5-EGFP$_{A20}$ retains a functional ability to mediate transduction through CAR (data not shown), the significant differences in genomes detected in the spleen or lung cannot be explained by differences in native receptor-mediated uptake. Warfarin pretreatment also reduced the accumulation of Ad5-EGFP$_{WT}$ (~9-fold; $P < 0.0001$) and Ad5-EGFP$_{A20}$ (~3-fold; $P = 0.003$) in the lung.

DISCUSSION

In this study we expanded the tropism of Ad5 to cells expressing αvβ6 integrin by genetically incorporating an αvβ6-

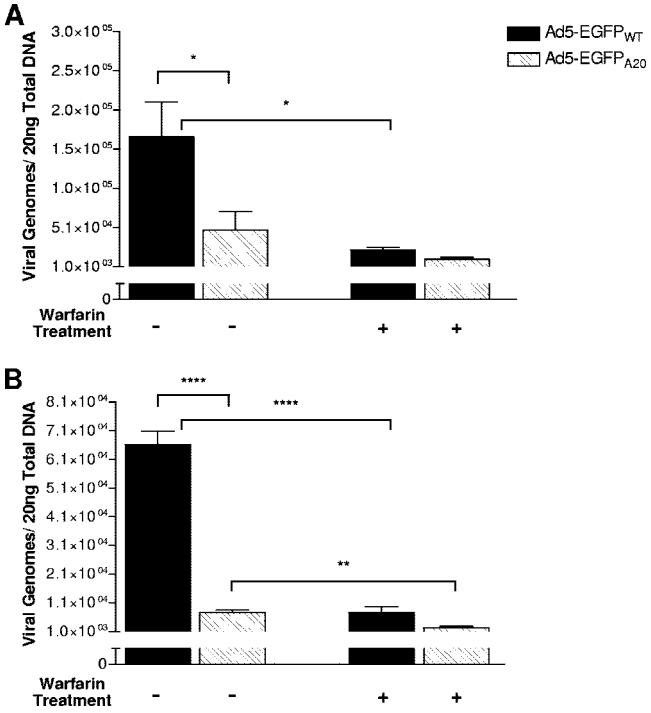

FIG. 6. Quantification of viral genomes in spleen and lung. CD1 nude female mice bearing DX3-β6 xenografts were administered either PBS, Ad5-EGFP$_{WT}$, or Ad5-EGFP$_{A20}$ (5×10^{10} vp/mouse) by intravenous tail vein injection without (−) or with (+) a predose of warfarin (133 μg) at days 3 and 1 prior to virus administration. Mice were killed after 72 h, necropsy performed, and DNA extracted from spleen (A) or lung (B) tissue. Absolute viral genomes were quantified by TaqMan real-time qPCR using a probe to detect the hexon region of the genome. Data represent the mean ± SEM ($n = 4$ or 5 mice) for triplicate samples. Statistical significance was determined using the unpaired Student t test comparing the means of two samples (*, $P < 0.05$; **, $P < 0.01$; ****, $P < 0.0001$).

targeting peptide, A20FMDV2, into the fiber knob domain. Studies using recombinant fiber knob protein (Knob$_{A20}$) demonstrated that the A20FMDV2 insertion within the HI loop remained functional, retaining its αvβ6 selectivity (Fig. 1A and B). In vitro, Ad5-EGFP$_{A20}$ showed superior CAR-independent delivery to all carcinoma lines used compared with Ad5-EGFP$_{WT}$, and we confirmed that the enhanced tropism was modulated through A20FMDV2 and was αvβ6 dependent. In vivo, systemic delivery of Ad5-EGFP$_{A20}$ resulted in enhanced tumor uptake. Furthermore, Ad5-EGFP$_{A20}$ displayed an altered distribution, with reduced uptake in the liver, spleen, and lung, and also was associated with significantly reduced vector-related toxicity.

With the aim of improving tumor delivery in vivo, various retargeting strategies have been described for adenoviruses. These have included the incorporation of an RGD-4C nonapeptide or polylysine (pK7) motif into the Ad5 fiber protein to allow RGD-dependent enhancement of CAR-negative cell lines that express αvβ3/5 integrins (12, 34) or improve infection of myeloma and glioma cells in vitro (17, 42). However, high-efficiency transduction in vitro does not always correlate with success in vivo, and it is worth noting that these retargeting strategies are designed to broadly enhance the tropism of Ad5 and are not cancer selective, a factor which must be considered when administering these vectors systemically. The rational retargeting approach undertaken in this study is selective for αvβ6. Importantly, αvβ6 already has been identified and assessed for its suitability as a tumor-specific cell surface molecule (1, 4, 7, 13, 35, 43, 44, 45, 46), and in addition, the highly potent A20FMDV2 peptide has previously been characterized with regard to its affinity and selectivity for its target, αvβ6 (10, 11).

We used the DX3-β6 xenograft model (low CAR and high αvβ6) to compare the tumor-targeting efficiencies of Ad5-EGFP$_{WT}$ and Ad5-EGFP$_{A20}$ following systemic delivery, and in a parallel experiment we assessed the effects of coagulation factor depletion on the uptake of both vectors in the tumor and liver. Using qPCR to quantify absolute viral genome numbers, we demonstrated a twofold increase in tumor uptake in the non-warfarin-treated Ad5-EGFP$_{A20}$ group compared with the Ad5-EGFP$_{WT}$ group. Unexpectedly, we found a reduction in the number of absolute genomes detected in the liver for Ad5-EGFP$_{A20}$ (~5-fold; $P = 0.0002$) compared with Ad5-EGFP$_{WT}$. Reduced genome levels in the liver correlated with decreased E1A expression and lower serum transaminase levels (ALT and AST), indicators of hepatotoxicity in vivo. Histologically the livers from mice treated with Ad5-EGFP$_{WT}$ showed hepatic injury and prominent hepatocyte necrosis (Fig. 4C), whereas there was markedly less cell damage evident in the Ad5-EGFP$_{A20}$ group, further supporting its reduced hepatotoxicity in vivo.

Vector clearance by the reticuloendothelial system, particularly by Kupffer cells, is a major limitation to systemic delivery of therapeutic adenoviruses in vivo. Recently, vitamin K-dependent zymogens have been shown to facilitate hepatocyte uptake, mediated through a direct Ad5 hexon-FX interaction (22, 48) promoting engagement with alternative receptors expressed in the liver, such as heparan sulfate proteoglycans or low-density lipoprotein receptor-related protein (41, 48). With the aim of increasing blood persistence and bioavailability for tumors in vivo, warfarin pretreatment can be used as a strategy to avoid liver transduction by depleting various coagulation factors. The success of this strategy has been controversial, with some reports of enhanced tumor uptake (40) and other reports of reductions in uptake (16). We observed a slight increase in the quantity of Ad5-EGFP$_{WT}$ genomes delivered to the tumor in warfarin-pretreated animals. However, the warfarin-pretreated Ad5-EGFP$_{A20}$ group exhibited an almost twofold reduction compared with the untreated cohort. Warfarin reduced liver uptake and hepatic toxicity significantly for both viruses used in this study. However, this effect was more apparent in the Ad5-EGFP$_{A20}$ group, where we observed a substantial decrease in vector genomes in the liver (~160-fold; $P = 0.035$), compared to only a ~9-fold reduction in the warfarin-treated Ad5-EGFP$_{WT}$ group ($P < 0.0001$). Both viruses were affected by warfarin pretreatment; however, these data suggest that Ad5-EGFP$_{A20}$ is more sensitive to the effects of warfarin in vivo, either through its direct effects on coagulation factors or through another, as-yet-unknown, mechanism.

In the absence of warfarin, Ad5-EGFP$_{A20}$ also displayed an altered biodistribution compared with Ad5-EGFP$_{WT}$, which resulted in significantly reduced splenic and pulmonary uptake, a profile which paralleled that for the warfarin-pretreated Ad5-

$EGFP_{WT}$ group. We detected approximately threefold- and ninefold-fewer Ad5-$EGFP_{A20}$ genomes in the spleens and lungs of non-warfarin-treated animals ($P = 0.046$ and $P < 0.0001$, respectively), organs previously described as auxiliary sites for Ad5 uptake (28). Interestingly, altered in vivo biodistribution already has been described for systemically delivered RGD-modified adenoviruses, albeit with increased levels of gene expression detected in the liver, spleen, and lung (39). However, such enhanced tropism in vivo would be consistent with the broad tissue distribution of αvβ3 and αvβ5 integrins, the target receptors for Ad5-RGD-4C (27). More recently, a biodistribution profile similar to that of Ad5-$EGFP_{A20}$ has been described for another fiber-modified adenovirus, Ad-K7-L2 which features a polylysine motif in the C terminus of the fiber knob domain (24). Those authors also reported reductions in liver toxicity, as measured by serum AST levels and histological examination, for Ad-K7-L2 compared with the conventional Ad5 control vector, a profile partially attributed to low-level interleukin-6 induction as a result of limited vector uptake in the spleen (24). As the spleen is a major site for the induction of innate immune responses following systemic delivery of adenovirus vectors, it has been proposed that vectors which have limited splenic accumulation would be safer vehicles for gene therapy applications (24, 53). Certainly, data obtained with Ad5-$EGFP_{A20}$ support this hypothesis; we also observed reduced toxicity and minimal hepatic damage with limited splenic sequestration compared with Ad5-$EGFP_{WT}$.

We can propose a number of possible explanations for the altered biodistribution of Ad5-$EGFP_{A20}$, particularly with regard to the reticuloendothelial system. It now is well established that adenovirus interactions with serum factors play a more significant role in vivo than conventional in vitro interactions with CAR and αvβ3/αvβ5 integrins (41, 48, 52). The sole structural modification within this vector is the insertion of 20 amino acids into the HI loop of the fiber knob, such that the altered hepatotropism observed is unlikely to be due to interference with FX-hexon binding. However, FIX and C4BP previously have been described to bind to the knob domain of Ad5 (41). Those authors described a mutant Ad5, ablated for binding to these serum factors, which displayed reduced hepatocyte transduction and hepatotoxicity in vivo and a failure to colocalize with Kupffer cells. Interestingly, the set of mutations described are in close proximity to the site of insertion of A20FMDV2, and so it is plausible that this modification has conferred a conformational change or steric hindrance which may abrogate FIX and/or C4BP binding to Ad5-$EGFP_{A20}$.

Alternatively, the insertion of the strongly cationic A20FMDV2 peptide (pI = 11.32) may well alter the overall electrostatic properties of the predominantly negative Ad5 particle in vivo (2), precluding uptake by scavenging receptors on KC, which preferentially recognize negatively charged materials (2, 14, 18). More recently, opsonization by complement (C3 and C4) in combination with natural IgM antibodies has been proposed as an alternative mechanism for the uptake of Ads by scavenging receptors on Kupffer cells in vivo (52). Interestingly, the electrostatic characteristics of Ad5 can also dictate the extent of recognition by serum proteins, including complement (9, 14).

Finally, we cannot eliminate the possibility that Ad5-$EGFP_{A20}$ is sequestered in other murine organs. The expression profile of αvβ6 in human tissue is well characterized, where it is restricted to epithelial remodeling events, such as embryogenesis, wound healing, and carcinogenesis (7). However, it is possible that murine epithelia may express the integrin, although we did not detect an increased accumulation of Ad5-$EGFP_{A20}$ relative to Ad5-$EGFP_{WT}$ in any of the murine organs analyzed in this study. Furthermore, it is important to note that the factors which dictate the in vivo biodistribution of nonretargeted Ad5 vectors are not well understood. Therefore, it will be interesting to compare the kinetics and biodistribution of viral uptake in vivo for both Ad5-$EGFP_{WT}$ and Ad5-$EGFP_{A20}$, especially at earlier time points.

Refining the therapeutic index is an important goal when designing adenovirus vectors for cancer therapy, especially for the treatment of disseminated disease. However, several challenges still remain. The recent finding that human but not murine erythrocytes express CAR (8) warrants consideration when developing relevant in vivo models for the study of intravenously delivered adenoviruses. The high-efficiency, CAR-independent transduction that we observed in vitro suggests that CAR binding, in the context of Ad5-$EGFP_{A20,}$ is dispensable. It will be of interest to determine if a CAR-ablated derivative of this construct proves useful in avoiding erythrocyte binding.

Prototype vectors with high affinity and selectivity for clinically important markers in vivo are highly desirable, as they will permit the reduction of the vector dose administered in vivo and therefore limit vector-related toxicity. In this study, using Ad5-$EGFP_{A20}$, we improved liver-to-tumor ratios (viral genomes) significantly, with non-warfarin-treated Ad5-$EGFP_{WT}$ and Ad5-$EGFP_{A20}$ groups having ratios of ~900:1 and ~100:1, respectively, and warfarin-treated Ad5-$EGFP_{WT}$ and Ad5-$EGFP_{A20}$ groups having significantly improved ratios of ~70:1 and 1:1, respectively. In summary, we have generated a retargeted virus, Ad5-$EGFP_{A20,}$ which displays improved tumor transduction in vivo and, in addition, shows significantly less toxicity through a naturally reduced tropism for the reticuloendothelial system.

ACKNOWLEDGMENTS

We thank Jennelle Francis, Jerome Burnet, Vipul Bhakta, and Linda Hammond for technical assistance and Nicola O Reilly and the Protein Isolation and Cloning Laboratory at the London Research Laboratories, CR-UK, for protein purification. We also thank Ramon Alemany and Manel Cascallo for helpful suggestions and discussions.

This research was supported by Cancer Research UK, St. Bartholomew's and The Royal London Charitable Foundation, and The Health Foundation.

REFERENCES

1. **Ahmed, N., C. Riley, G. E. Rice, M. A. Quinn, and M. S. Baker.** 2002. Alpha(v) beta(6) integrin—a marker for the malignant potential of epithelial ovarian cancer. J. Histochem. Cytochem. **50:**1371–1380.
2. **Alemany, R., K. Suzuki, and D. T. Curiel.** 2000. Blood clearance rates of adenovirus type 5 in mice. J. Gen. Virol. **81:**2605–2609.
3. **Anders, M., M. Vieth, C. Röcken, M. Ebert, M. Pross, S. Gretschel, P. M. Schlag, B. Wiedenmann, W. Kemmner, and M. Höcker.** 2009. Loss of the coxsackie and adenovirus receptor contributes to gastric cancer progression. Br. J. Cancer **100:**352–359.
4. **Bates, R. C.** 2005. Colorectal cancer progression: integrin alphavbeta6 and the epithelial-mesenchymal transition (EMT). Cell Cycle **4:**1350–1352.
5. **Belousova, N., V. Krendelchtchikova, D. T. Curiel, and V. Krasnykh.** 2002. Modulation of adenovirus vector tropism via incorporation of polypeptide ligands into the fiber protein. J. Virol. **76:**8621–8631.
6. **Bergelson, J. M., A. Krithivas, L. Celi, G. Droguett, M. S. Horwitz, T. Wickham, R. L. Crowell, and R. W. Finberg.** 1998. The murine CAR ho-

molog is a receptor for coxsackie B viruses and adenoviruses. J. Virol. **72:**415–419.
7. **Breuss, J., J. Gallo, H. DeLisser, I. Klimanskaya, H. Folkesson, J. Pittet, S. Nishimura, K. Aldape, D. Landers, W. Carpenter, N. Gillett, D. Sheppard, M. Matthay, S. Albelda, R. Kramer, and R. Pytela.** 1995. Expression of the beta 6 integrin subunit in development, neoplasia and tissue repair suggests a role in epithelial remodeling. J. Cell Sci. **108:**2241–2251.
8. **Carlisle, R. C., Y. Di, A. M. Cerny, A. F. Sonnen, R. B. Sim, N. K. Green, V. Subr, K. Ulbrich, R. J. Gilbert, K. D. Fisher, R. W. Finberg, and L. W. Seymour.** 2009. Human erythrocytes bind and inactivate type 5 adenovirus by presenting coxsackievirus-adenovirus receptor and complement receptor 1. Blood **113:**1909–1918.
9. **Chonn, A., P. R. Cullis, and D. V. Devine.** 1991. The role of surface charge in the activation of the classical and alternative pathways of complement by liposomes. J. Immunol. **146:**4234–4241.
10. **DiCara, D., C. Rapisarda, J. L. Sutcliffe, S. M. Violette, P. H. Weinreb, I. R. Hart, M. J. Howard, and J. F. Marshall.** 2007. Structure-function analysis of Arg-Gly-Asp helix motifs in alpha v beta 6 integrin ligands. J. Biol. Chem. **282:**9657–9665.
11. **Dicara, D., A. Burman, S. Clark, S. Berryman, M. J. Howard, I. R. Hart, J. F. Marshall, and T. Jackson.** 2008. Foot-and-mouth disease virus forms a highly stable, EDTA-resistant complex with its principal receptor, integrin αvβ6: implications for infectiousness. J. Virol. **82:**1537–1546.
12. **Dmitriev, I., V. Krasnykh, C. R. Miller, M. Wang, E. Kashentseva, G. Mikheeva, N. Belousova, and D. T. Curiel.** 1998. An adenovirus vector with genetically modified fibers demonstrates expanded tropism via utilization of a coxsackievirus and adenovirus receptor-independent cell entry mechanism. J. Virol. **72:**9706–9713.
13. **Elayadi, A. N., K. N. Samli, L. Prudkin, Y. H. Liu, A. Bian, X. J. Xie, I. I. Wistuba, J. A. Roth, M. J. McGuire, and K. C. Brown.** 2007. A peptide selected by biopanning identifies the integrin alphavbeta6 as a prognostic biomarker for nonsmall cell lung cancer. Cancer Res. **67:**5889–5895.
14. **Furumoto, K., S. Nagayama, K. Ogawara, Y. Takakura, M. Hashida, K. Higaki, and T. Kimura.** 2004. Hepatic uptake of negatively charged particles in rats: possible involvement of serum proteins in recognition by scavenger receptor. J. Control Release **97:**133–141.
15. **Gagnebin, J., M. Brunori, M. Otter, L. Juillerat-Jeanneret, P. Monnier, and R. Iggo.** 1999. A photosensitising adenovirus for photodynamic therapy. Gene Ther. **6:**1742–1750.
16. **Gimenez-Alejandre, M., M. Cascallo, N. Bayo-Puxan, and R. Alemany.** 2008. Coagulation factors determine tumor transduction *in vivo.* Hum. Gene Ther. **19:**1415–1419.
17. **Gonzalez, R., R. Vereecque, T. J. Wickham, T. Facon, D. Hetuin, I. Kovesdi, F. Bauters, P. Fenaux, and B. Quesnel.** 1999. Transduction of bone marrow cells by the AdZ.F(pK7) modified adenovirus demonstrates preferential gene transfer in myeloma cells. Hum. Gene Ther. **10:**2709–2717.
18. **Haisma, H., J. Kamps, G. Kamps, J. Plantinga, M. Rots, and A. Bellu.** 2008. Polyinosinic acid enhances delivery of adenovirus vectors *in vivo* by preventing sequestration in liver macrophages J. Gen. Virol. **89:**1097–1105.
19. **Hawkins, L. K., L. Johnson, M. Bauzon, J. A. Nye, D. Castro, G. A. Kitzes, M. D. Young, J. K. Holt, P. Trown, and T. W. Hermiston.** 2001. Gene delivery from the E3 region of replicating human adenovirus: evaluation of the 6.7 K/gp19 K region. Gene Ther. **8:**1123–1131.
20. **Jackson, T., D. Sheppard, M. Denyer, W. Blakemore, and A. M. King.** 2000. The epithelial integrin αvβ6 is a receptor for foot-and-mouth disease virus. J. Virol. **74:**4949–4956.
21. **Jee, Y. S., S. G. Lee, J. C. Lee, M. J. Kim, J. J. Lee, D. Y. Kim, S. W. Park, M. W. Sung, and D. S. Heo.** 2002. Reduced expression of coxsackievirus and adenovirus receptor (CAR) in tumor tissue compared to normal epithelium in head and neck squamous cell carcinoma patients. Anticancer Res. **22:**2629–2634.
22. **Kalyuzhniy, O., N. C. Di Paolo, M. Silvestry, S. E. Hofherr, M. A. Barry, P. L. Stewart, and D. M. Shayakhmetov.** 2008. Adenovirus serotype 5 hexon is critical for virus infection of hepatocytes *in vivo*. Proc. Natl. Acad. Sci. USA **105:**5483–5488.
23. **Kirby, I., E. Davison, A. J. Beavil, C. P. Soh, T. J. Wickham, P. W. Roelvink, I. Kovesdi, B. J. Sutton, and G. Santis.** 2000. Identification of contact residues and definition of the CAR-binding site of adenovirus type 5 fiber protein. J. Virol. **74:**2804–2813.
24. **Koizumi, N., T. Yamaguchi, K. Kawabata, F. Sakurai, T. Sasaki, Y. Watanabe, T. Hayakawa, and H. Mizuguchi.** 2007. Fiber-modified adenovirus vectors decrease liver toxicity through reduced IL-6 production. J. Immunol. **178:**1767–1773.
25. **Krasnykh, V. N., G. V. Mikheeva, J. T. Douglas, and D. T. Curiel.** 1996. Generation of recombinant adenovirus vectors with modified fibers for altering viral tropism. J. Virol. **70:**6839–6846.
26. **Kurachi, S., K. Tashiro, F. Sakurai, H. Sakurai, K. Kawabata, K. Yayama, H. Okamoto, S. Nakagawa, and H. Mizuguchi.** 2007. Fiber-modified adenovirus vectors containing the TAT peptide derived from HIV-1 in the fiber knob have efficient gene transfer activity. Gene Ther. **14:**1160–1165.
27. **Lord, R., M. Parsons, I. Kirby, A. Beavil, J. Hunt, B. Sutton, and G. Santis.** 2006. Analysis of the interaction between RGD-expressing adenovirus type 5 fiber knob domains and alphavbeta3 integrin reveals distinct binding profiles and intracellular trafficking. J. Gen. Virol. **87:**2497–2505.
28. **Manickan, E., J. S. Smith, J. Tian, T. L. Eggerman, J. N. Lozier, J. Muller, and A. P. Byrnes.** 2006. Rapid Kupffer cell death after intravenous injection of adenovirus vectors. Mol. Ther. **13:**108–117.
29. **Marshall, J. F., S. A. Nesbitt, M. H. Helfrich, M. A. Horton, K. Polakova, and I. R. Hart.** 1991. Integrin expression in human melanoma cell lines: heterogeneity of vitronectin receptor composition and function. Int. J. Cancer. **49:**924–931.
30. **Matsumoto, K., S. F. Shariat, G. E. Ayala, K. A. Rauen, and S. P. Lerner.** 2005. Loss of coxsackie and adenovirus receptor expression is associated with features of aggressive bladder cancer. Urology **66:**441–446.
31. **Merron, A., I. Peerlinck, P. Martin-Duque, J. Burnet, M. Quintanilla, S. Mather, M. Hingorani, K. Harrington, R. Iggo, and G. Vassaux.** 2007. SPECT/CT imaging of oncolytic adenovirus propagation in tumours *in vivo* using the Na/I symporter as a reporter gene. Gene Ther. **14:**1731–1738.
32. **Mikami, T., K. Ookawa, T. Shimoyama, S. Fukuda, H. Saito, and A. Munakata.** 2001. KAI1, CAR, and Smad4 expression in the progression of colorectal tumor. J. Gastroenterol. **36:**465–469.
33. **Munger, J. S., X. Huang, H. Kawakatsu, M. J. Griffiths, S. L. Dalton, J. Wu, J. F. Pittet, N. Kaminski, C. Garat, M. A. Matthay, D. B. Rifkin, and D. Sheppard.** 1999. The integrin alpha v beta 6 binds and activates latent TGF beta 1: a mechanism for regulating pulmonary inflammation and fibrosis. Cell **96:**319–328.
34. **Nagel, H., S. Maag, A. Tassis, F. O. Nestlé, U. F. Greber, and S. Hemmi.** 2003. The alphavbeta5 integrin of hematopoietic and nonhematopoietic cells is a transduction receptor of RGD-4C fiber-modified adenoviruses. Gene Ther. **10:**1643–1653.
35. **Nystrom, M. L., D. McCulloch, P. H. Weinreb, S. M. Violette, P. M. Speight, J. F. Marshall, I. R. Hart, and G. J. Thomas.** 2006. Cyclooxygenase-2 inhibition suppresses alphavbeta6 integrin-dependent oral squamous carcinoma invasion. Cancer Res. **66:**10833–10842.
36. **Parker, A. L., S. N. Waddington, C. G. Nicol, D. M. Shayakhmetov, S. M. Buckley, L. Denby, G. Kemball-Cook, S. Ni, A. Lieber, J. H. McVey, S. A. Nicklin, and A. H. Baker.** 2006. Multiple vitamin K-dependent coagulation zymogens promote adenovirus-mediated gene delivery to hepatocytes. Blood **108:**2554–2561.
37. **Rauen, K. A., D. Sudilovsky, J. L. Le, K. L. Chew, B. Hann, V. Weinberg, L. D. Schmitt, and F. McCormick.** 2002. Expression of the coxsackie adenovirus receptor in normal prostate and in primary and metastatic prostate carcinoma: potential relevance to gene therapy. Cancer Res. **62:**3812–3818.
38. **Reed, L. J., and H. Muench.** 1938. A simple method for estimating fifty percent endpoints. Am. J. Hyg. **27:**493–497.
39. **Reynolds, P., I. Dmitriev, and D. Curiel.** 1999. Insertion of an RGD motif into the HI loop of adenovirus fiber protein alters the distribution of transgene expression of the systemically administered vector. Gene Ther. **6:**1336–1339.
40. **Shashkova, E. V., K. Doronin, J. S. Senac, and M. A. Barry.** 2008. Macrophage depletion combined with anticoagulant therapy increases therapeutic window of systemic treatment with oncolytic adenovirus. Cancer Res. **68:**5896–5904.
41. **Shayakhmetov, D. M., A. Gaggar, S. Ni, Z. Y. Li, and A. Lieber.** 2005. Adenovirus binding to blood factors results in liver cell infection and hepatotoxicity. J. Virol. **79:**7478–7491.
42. **Staba, M. J., T. J. Wickham, I. Kovesdi, and D. E. Hallahan.** 2000. Modifications of the fiber in adenovirus vectors increase tropism for malignant glioma models. Cancer Gene Ther. **7:**13–19.
43. **Thomas, G. J., M. P. Lewis, S. A. Whawell, A. Russell, D. Sheppard, I. R. Hart, P. M. Speight, and J. F. Marshall.** 2001. Expression of the alphavbeta6 integrin promotes migration and invasion in squamous carcinoma cells. J. Investig. Dermatol. **117:**67–73.
44. **Thomas, G. J., I. R. Hart, P. M. Speight, and J. F. Marshall.** 2002. Binding of TGF-beta1 latency-associated peptide (LAP) to alpha(v)beta6 integrin modulates behaviour of squamous carcinoma cells. Br. J. Cancer **87:**859–867.
45. **Thomas, G. J., M. L. Nyström, and J. F. Marshall.** 2006. Alphavbeta6 integrin in wound healing and cancer of the oral cavity. J. Oral Pathol. Med. **35:**1–10.
46. **Van Aarsen, L. A., D. R. Leone, S. Ho, B. M. Dolinski, P. E. McCoon, D. J. LePage, R. Kelly, G. Heaney, P. Rayhorn, C. Reid, K. J. Simon, G. S. Horan, N. Tao, H. A. Gardner, M. M. Skelly, A. M. Gown, G. J. Thomas, P. H. Weinreb, S. E. Fawell, and S. M. Violette.** 2008. Antibody-mediated blockade of integrin alpha v beta 6 inhibits tumor progression *in vivo* by a transforming growth factor-beta-regulated mechanism. Cancer Res. **68:**561–570.
47. **Vassaux, G., A. L. Manson, and C. Huxley.** 1997. Copy number-dependent expression of a YAC-cloned human CFTR gene in a human epithelial cell line. Gene Ther. **4:**618–623.
48. **Waddington, S. N., J. H. McVey, D. Bhella, A. L. Parker, K. Barker, H. Atoda, R. Pink, S. M. Buckley, J. A. Greig, L. Denby, J. Custers, T. Morita, I. M. Francischetti, R. Q. Monteiro, D. H. Barouch, N. van Rooijen, C. Napoli, M. J. Havenga, S. A. Nicklin, and A. H. Baker.** 2008. Adenovirus serotype 5 hexon mediates liver gene transfer. Cell **132:**397–409.

49. **Wickham, T. J., P. Mathias, D. A. Cheresh, and G. R. Nemerow.** 1993. Integrins alpha v beta 3 and alpha v beta 5 promote adenovirus internalization but not virus attachment. Cell **73:**309–319.
50. **Wickham, T. J., E. Tzeng, L. L. Shears II, P. W. Roelvink, Y. Li, G. M. Lee, D. E. Brough, A. Lizonova, and I. Kovesdi.** 1997. Increased in vitro and in vivo gene transfer by adenovirus vectors containing chimeric fiber proteins. J. Virol. **71:**8221–8229.
51. **Xia, D., L. Henry, R. D. Gerard, and J. Deisenhofer.** 1995. Structure of the receptor binding domain of adenovirus type 5 fiber protein. Curr. Top. Microbiol. Immunol. **199:**39–46.
52. **Xu, Z., J. Tian, J. S. Smith, and A. P. Byrnes.** 2008. Clearance of adenovirus by Kupffer cells is mediated by scavenger receptors, natural antibodies, and complement. J. Virol. **82:**11705–11713.
53. **Zhang, Y., N. Chirmule, G. P. Gao, R. Qian, M. Croyle, B. Joshi, J. Tazelaar, and J. M. Wilson.** 2001. Acute cytokine response to systemic adenoviral vectors in mice is mediated by dendritic cells and macrophages. Mol. Ther. **3:**697–707.